

RAPID COMMUNICATION

Hollow nanospheres of mesoporous Co_9S_8 as a high-capacity and long-life anode for advanced lithium ion batteries

Yanli Zhou^a, Dong Yan^a, Huayun Xu^a, Jinkui Feng^b, Xiaolei Jiang^a, Jie Yue^a, Jian Yang^{a,*}, Yitai Qian^{a,c}



^aKey Laboratory of Colloid and Interface Chemistry, Ministry of Education School of Chemistry and Chemical Engineering, Shandong University, Jinan 250100, PR China

^bSchool of Material Science and Engineering, Shandong University Jinan 250061, PR China

^cHefei National Laboratory for Physical Science at Microscale, Department of Chemistry, University of Science and Technology of China, Hefei 230026, PR China

Received 2 October 2014; received in revised form 27 December 2014; accepted 8 January 2015

Available online 15 January 2015

KEYWORDS

Nanomaterials;
Hollow structures;
Electrochemical properties;
Lithium ion batteries

Abstract

Hollow nanospheres of mesoporous Co_9S_8 are successfully synthesized by a facile solvothermal reaction followed with a high-temperature annealing in Ar/H_2 . These hollow nanoparticles exhibit a reversible capacity of $\sim 1414 \text{ mA h g}^{-1}$ after 100 cycles at 100 mA g^{-1} . In the course of this cycling, there is a significant capacity recovery, which is associated with enhanced capacitance caused by repeated electro-chemical milling. The growth of a carbon shell on the hollow nanospheres further improves the reversible capacities at high rates, $\sim 896 \text{ mA h g}^{-1}$ after 800 cycles at 2 A g^{-1} . The excellent lithium-storage performances shed light on the promising potential of sulfides as a high capacity, high rate and long life anodes.

© 2015 Elsevier Ltd. All rights reserved.

Introduction

Lithium ion batteries (LIBs) as one of the most promising energy storage systems, have been successfully applied in a variety of portable electronic devices and electric vehicles

(EVs) [1,2], due to high energy density, light weight and long cycle life. Though graphite as a commercial anode achieves great successes, it is still limited by its low theoretical capacity and safety issues [3]. Thus, great efforts have been devoted to searching new materials as next-generation anodes. Transitional metal sulfides are turning into one of these alternative materials [4–8], because of their high theoretical capacities, low cost and large abundance in the world. But they have to face the challenges from huge volume changes upon cycling,

*Corresponding author. Tel.: +86 531 88364489.
E-mail address: yangjian@sdu.edu.cn (J. Yang).

which easily lead to cracking, fracture and electrical disconnection of electrodes. These serious concerns on sulfides could be addressed by structure engineering and carbon coating, which are already well demonstrated in transitional metal oxides [9-14], but less in sulfides.

Cobalt sulfides as an anode have been receiving attention recently, due to their high electronic conductivity, good thermal stability and high theoretical capacity [7,15-28]. For instance, rose-like Co₉S₈ architectures composed of randomly dispersed nano-sheets [17], presented a reversible capacity of 123 mA h g⁻¹ after 30 cycles at 50 mA g⁻¹. This capacity was promoted to ~302 mA h g⁻¹ by flower-like CoS micro-particles obtained by a solvothermal reaction [18]. Yolk-shell microspheres of Co₉S₈ prepared by spray pyrolysis and high-temperature sulfidation, further enhanced the reversible capacity to 634 mA h g⁻¹ for 100 cycles at 1 A g⁻¹ [19]. Surface modification of sulfides by carbon is another way to improve electrochemical performances. This strategy was exemplified by dandelion-like Co₉S₈@C nanostructures [7]. The specific capacity could be maintained at 520 mA h g⁻¹ over 50 cycles at a current density of 1 A g⁻¹. Graphene-wrapped CoS nanoparticles synthesized with graphene oxide as a reagent, delivered a specific capacity of 749 mA h g⁻¹ after 40 cycles at 62.5 mA g⁻¹ or ~550 mA h g⁻¹ after 100 cycles at 312.5 mA g⁻¹ [20]. So far, these combinations of structure engineering and carbon coating for cobalt sulfides do not realize the satisfied performances yet, due to lack of effective controls on size and structure.

Herein, hollow nanospheres of mesoporous Co₉S₈ are successfully synthesized by a simple solvothermal reaction followed by a high-temperature calcination in Ar/H₂. Electrochemical measurements show their outstanding lithium-storage performance, ~1414 mA h g⁻¹ after 100 cycles at a current density of 100 mA g⁻¹. This result is much higher than those in literature [15-28]. Intriguingly, the cycling of these hollow nanospheres presents a typical capacity recovery, which was observed in many transitional metal oxides but less understood [11,14,29]. Thus, discharge-charge and CV measurements are conducted to shed light on the nature of this capacity recovery using Co₉S₈ as a model. Finally, the long-term cycling of hollow nanospheres of mesoporous Co₉S₈ at high rates could be further enhanced by carbon coating. After this coating, the specific capacity could be kept at 896 mA h g⁻¹ over 800 cycles at 2 A g⁻¹, which is the best result for cobalt sulfides to our knowledge.

Experimental section

Preparation of hollow nanospheres of mesoporous Co₉S₈

All the chemicals were analytical grade without further purification. In a typical procedure, 1.5 mmol of cobalt acetate tetrahydrate (Co(Ac)₂·4H₂O) and 4.5 mmol of thiourea (Tu) were added to 50 mL ethylene glycol (EG), and then were stirred at room temperature for 0.5 h to form a pink solution. The solution was transferred into a Teflon-lined stainless steel autoclave with a capacity of 80 mL. The autoclave was sealed and maintained at 200 °C for 24 h. The resultant hollow nanospheres of CoS₂ were rinsed with deionized water and absolute alcohol for several times, and dried in an oven at 80 °C. Finally,

this product was annealed at 650 °C for 5 h in Ar/H₂, producing hollow nanospheres of mesoporous Co₉S₈.

Sample characterization

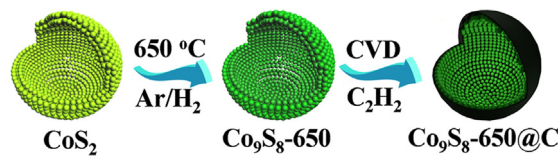
Powder X-ray diffraction (XRD) patterns were obtained by a Bruker D8 advanced X-ray diffractometer equipped with graphite-monochromatized Cu K α radiation ($\lambda=1.5418\text{ \AA}$). Transmission electron microscope (TEM) images, high-resolution transmission electron microscope (HRTEM) images, energy-dispersive X-ray spectra (EDS) as well as selected area electron diffraction (SAED) patterns were recorded on a high-resolution transmission electron microscope (JEOL-2100, Japan) at an acceleration voltage of 200 kV. Scanning electron microscope (SEM) images were acquired from a field-emission scanning electron microscope (SUPRA™ 55, German). X-ray photoelectron spectra (XPS) were obtained on an ESCALAB 250 spectrometer (ThermoFisher Sci., USA). The binding energies are corrected by C 1s at 284.60 eV. Nitrogen sorption isotherm was performed at 77.3 K on a Micromeritics ASAP2020HD88 gas sorptometer (Micromeritics, USA). Raman spectra were measured by a confocal MicroRaman spectrometer with an excitation wavelength of 515 nm (Olympus FV500, Japan).

Electrochemical measurements

Electrochemical properties of the samples were measured by CR2032 coin cells. To prepare the working electrode, a mixture of 70 wt% of active material, 20 wt% of acetylene black, and 10 wt% of CMC (carboxyl methyl cellulose) in deionized water was pasted on a clean copper foil and then dried in vacuum at 60 °C for 10 h. The resulting foil was roll-pressed and punched into discs. The mass loading of the active material is about 1.0 mg cm⁻². The cells were assembled in an argon-filled glovebox, by using a lithium foil as the counter electrode, a Celgard 2400 microporous polypropylene membrane as the separator, and a solution of 1 M LiPF₆ in ethylene carbonate (EC) and dimethyl carbonate (DMC) (1:1 v/v) as the electrolyte. Then, discharge and charge tests of the cells were carried out in the range of 0.01-3 V on battery cyclers (Land CT2001A, China). Electrochemical impedance spectra (EIS) were measured on an electrochemical workstation (Materials Mates 510, Italy) over a frequency range of 100 kHz to 0.01 Hz with an amplitude of 10 mV. Cyclic voltammetry (CV) curves were obtained from an electrochemical workstation (LK2005A, China) over 0.01-3 V at a scanning rate of 0.1 mV s⁻¹. All the electrochemical tests were carried out at 25 °C.

Results and discussion

The synthesis of hollow nanospheres of Co₉S₈@C could be briefly summarized by Scheme 1. First, cobalt acetate reacts



Scheme 1 Synthesis process of the hollow nanospheres of Co₉S₈-650@C.

with thiourea in ethylene glycol at 200 °C for 24 h, producing hollow nanospheres of CoS_2 . The absence of diffraction peaks in the XRD pattern (Figure S1) suggests the amorphous nature of CoS_2 . In spite of this, the formation of CoS_2 could be confirmed by EDS and XPS spectra. As shown in Figure S2, there are only Co and S in the products, beside C and Cu from the copper grid. The atomic ratio of Co to S is approximately 1:2, close to the stoichiometric ratio of CoS_2 . In the XPS spectra (Figure 1a), the strong binding energies at 778.5 and 793.6 eV are attributed to Co 2p_{3/2} and Co 2p_{1/2} from cobalt sulfides [30-32]. The shoulders at 780.5 and 797.3 eV are related to Co 2p_{3/2} and Co 2p_{1/2} from Co-O, due to the exposure of the product in air [33-35]. The weak binding energies centered around 784.2 and 802.2 eV could be identified as the shake-up peaks of Co^{2+} [31,36]. In the case of S, the intense binding energies at 161.5 and 162.6 eV (Figure 1b) are assigned to S 2p_{3/2} and S 2p_{1/2} from S^{2-} adsorbed on the surface [36]. While those at 162.4 and 163.5 eV agree well with the positions of disulfide species (S_2^{2-}) [37]. All the results indicate the formation of amorphous CoS_2 . SEM images show that amorphous CoS_2 comprises a large number of aggregated nanospheres with their sizes in the range of 120-400 nm (Figure 1c). These nanospheres exhibit cracking surfaces, which would benefit the penetration of electrolyte into active materials and promote the diffusion kinetics of lithium. Some of the nanospheres are broken, exposing their hollow interiors. The high-yield of hollow CoS_2

nanospheres is evidenced by the significant contrast difference in TEM images (Figure 1d). The formation of hollow structures is likely related to Kirkendall effect, because of unique yolk-shell structures in the intermediates (Figure S3).

Then, the hollow nanospheres of amorphous CoS_2 are calcined at 650 °C for 5 h in Ar/H₂ to convert to Co_9S_8 (Scheme 1). As shown in Figure 2a, the XRD pattern of the product after the calcination could be indexed as cubic-phase Co_9S_8 (JCPDS Card, No. 65-1765). TEM image shows that the resultant Co_9S_8 inherits the hollow structure from amorphous CoS_2 (Figure 2b), reflecting the good thermal stability of the hollow structure. The gaps between the neighboring primary particles make the shell highly porous (Figure 2c). SAED pattern of these hollow nanospheres (Figure 2d) consists of several bright diffraction rings, indicating the polycrystalline nature of the hollow Co_9S_8 nanospheres. This result could be ascribed to the random orientation of the primary particles in the shell, which is also supported by HRTEM images (Figure 2e). For the sake of clarity, the hollow nanospheres of mesoporous Co_9S_8 are denoted as Co_9S_8 -650 from now on.

The porous nature of the shell in the hollow nanospheres has been confirmed by N₂ sorption isotherms. As shown in Figures 3a and b, the hollow nanospheres of CoS_2 and Co_9S_8 -650 exhibit similar sorption curves, which could be identified as a type-IV isotherm with a small hysteresis in the range of P/P₀ over 0.8-1.0. This result indicates the mesoporous structure in the product, consistent with what observed in TEM images. The

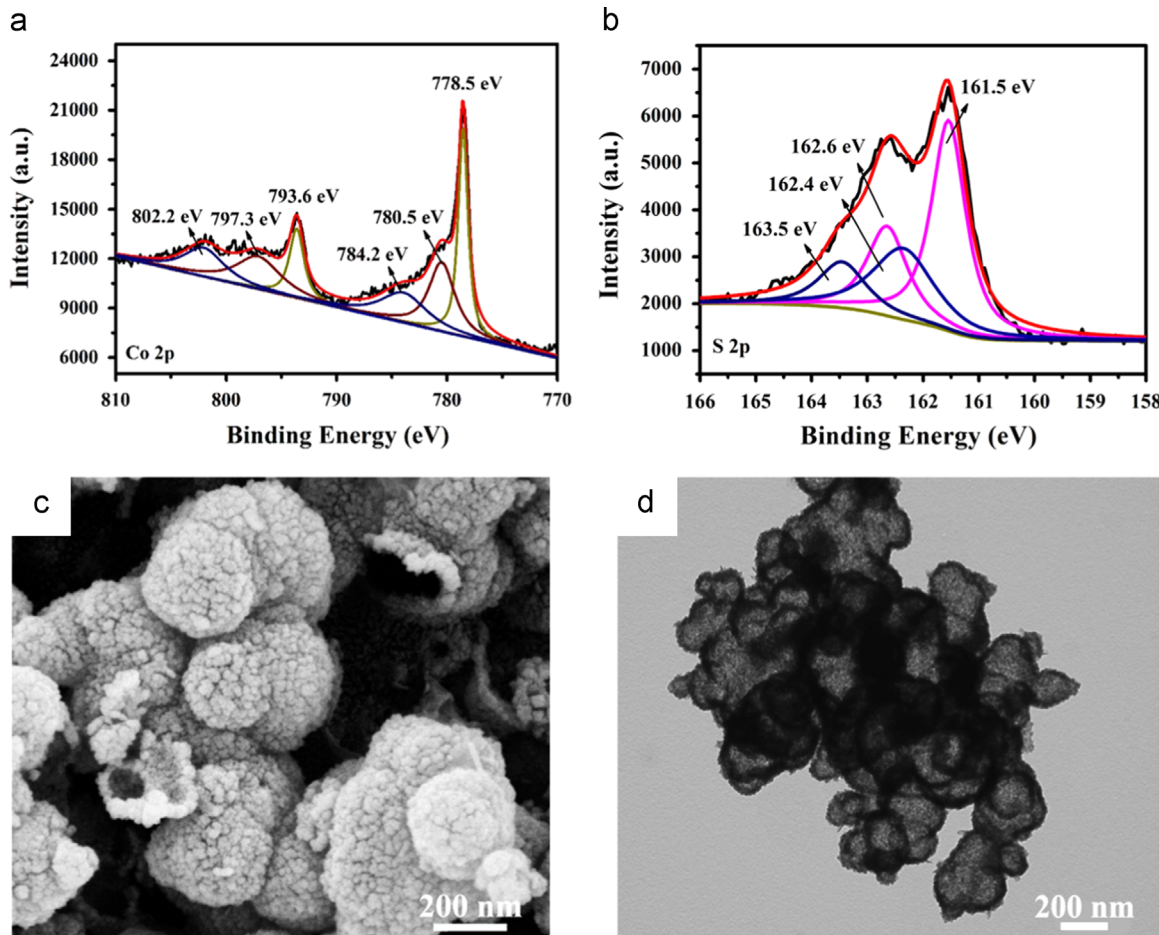


Figure 1 (a,b) XPS spectra, (c) SEM and (d) TEM images of the hollow nanospheres of amorphous CoS_2 .

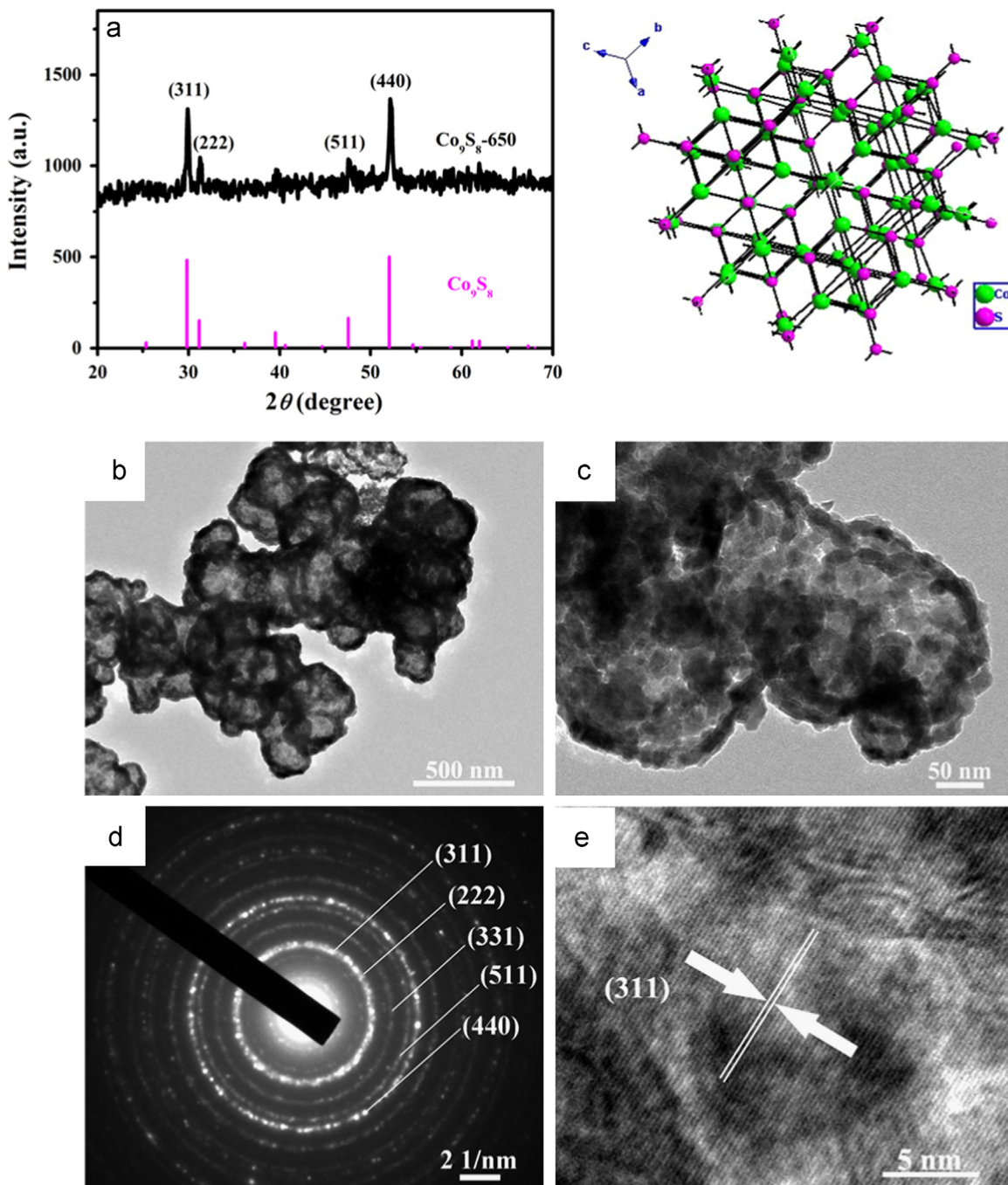


Figure 2 (a) XRD pattern of the product obtained by the calcination of the hollow nanospheres of amorphous CoS₂ at 650 °C, denoted as Co₉S₈-650. The bottom columns are the standard reflections of cubic-phase Co₉S₈, and the right figure is the corresponding crystal structure. (b,c) TEM images, (d) SAED pattern and (e) HRTEM image of hollow nanospheres of Co₉S₈-650.

pore size and specific surface area of the hollow nanospheres, decrease from 38 nm and 71.6 m² g⁻¹ of CoS₂ to 27 nm and 26.0 m² g⁻¹ of Co₉S₈-650 (Figures 3c and d), which could be attributed to the crystal growth of the primary particles in the shell, due to the high-temperature calcination.

The electrochemical properties of the hollow nanospheres of CoS₂ and Co₉S₈-650 are evaluated by cyclic voltammetry between 0.01 and 3 V at a scan rate of 0.1 mV s⁻¹, with Li foil as a counter and reference electrode. Figure 4a shows the CV profiles of the hollow nanospheres of CoS₂ for the first four

cycles. During the first cathodic scan, the reduction peak centered at 1.3 V could be ascribed to the intercalation of lithium into CoS₂ and the formation of Li_xCoS₂. The intense peak located around 1.1 V is indicative of the conversion of Li_xCoS₂ into metallic Co and the formation of Li₂S [15,17]. Additionally, there is a weak and broad peak at 0.7 V, which is believed to come from the formation of a solid electrolyte interphase (SEI) film [21]. The first anodic scan exhibits three peaks at 1.3, 2.1 and 2.4 V, corresponding to the oxidation of the above products [7]. In the subsequent scans, the cathodic

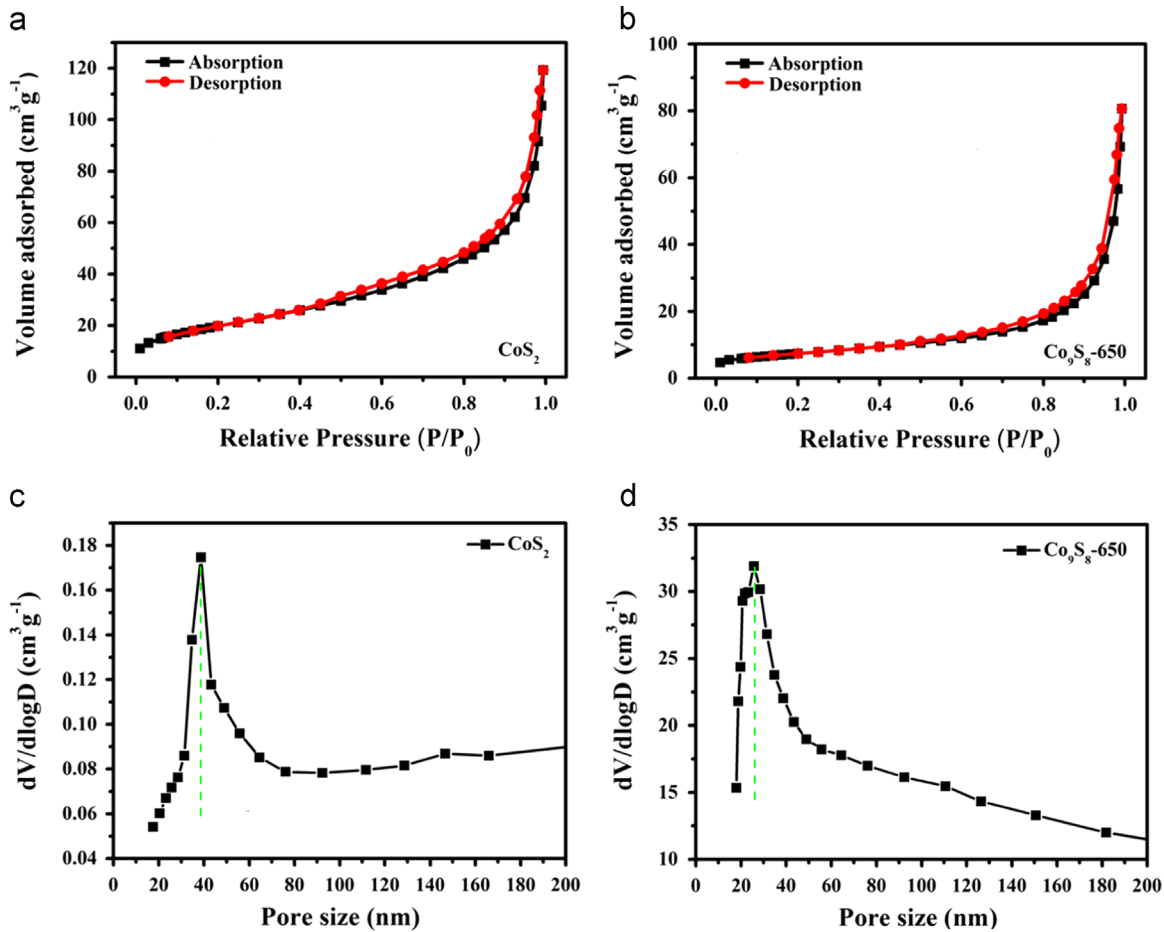


Figure 3 N₂ adsorption-desorption isotherm and pore size distribution of the hollow nanospheres of (a,b) CoS₂ and (c,d) Co₉S₈-650, respectively.

and anodic peaks shift toward the positive voltages, which might be caused by the irreversible structural changes triggered by the repeated reducing/oxidizing [38-40]. Meanwhile, the feature related with the SEI film gradually disappears from the CV profiles. Compared with the case of CoS₂, the CV profiles of Co₉S₈-650 (Figure 4b) are much simplified, in which the strong cathodic peak at 1.0 V is assigned to the reduction of Co₉S₈ to metallic Co [7]. The anodic peak at 2.0-2.1 V is ascribed to the sulfuration of metallic Co. The subsequent scans almost overlap with each other, indicating the good reversibility of the electrodes.

The first discharge/charge profiles of CoS₂ and Co₉S₈-650 are measured in the voltage range of 0.01-3.0 V at 100 mA g⁻¹. As shown in Figure 4c, the first discharge capacity of the hollow nanospheres of CoS₂ is ~1584 mA h g⁻¹, far beyond its theoretical capacity (~870 mA h g⁻¹) based on the conversion reaction. This result could be explained by the formation of the SEI film, the insertion of lithium into conductive carbon black, interfacial storage, etc [41]. The first charge profile exhibits a specific capacity of 987 mA h g⁻¹, corresponding to a coulombic efficiency of 62.3%. The large irreversible capacity is related to irreversible reactions upon cycling, such as the formation of a SEI film, the trapping of lithium inside the active material, the electrolyte decomposition catalyzed by Co, and so on [42-44]. The coulombic efficiency of the first cycle increases to 79.1% for Co₉S₈-650, in view of the first discharge at 1267 mA h g⁻¹ and

the first charge at 1002 mA h g⁻¹. This result could be assigned to the reduced specific area, which lowers the irreversible capacities from surface-related side reactions.

The cycling performances of the hollow nanospheres of CoS₂ and Co₉S₈-650 are evaluated over 0.01-3.0 V at a rate of 100 mA g⁻¹. As shown in Figure 4d, the reversible capacity of CoS₂ drops to only ~270 mA h g⁻¹ after 70 cycles, which is usually attributed to severe pulverization of electrode materials [6]. Co₉S₈-650 exhibits a totally different cycling performance from CoS₂. After the initial fading, the specific capacity gradually increases and then levels off at ~1400 mA h g⁻¹ at 100th cycle. Although the similar capacity recovery has been documented for many nanostructured oxides [11,29], there are still arguments about this origin. Huang and Hu attributed the capacity recovery in MnO to further oxidation of Mn²⁺ to high valence status (Mn³⁺ or Mn⁴⁺) above 2.0 V [10], which was supported by the anodic peak in the CV profiles and the shallow plateau in the charge curve. Another prevailing explanation is the repeated growth/dissolution of a gel-like polymer film [45], which also happens to the voltage above 2.0 V. Very recently, Lian et al. revisited the similar capacity recovery in Co₃O₄ and attributed it to self-reconstruction of active materials and SEI films [46]. Unfortunately, how to understand the nature of this capacity recovery in a view point of electrochemistry is still missed.

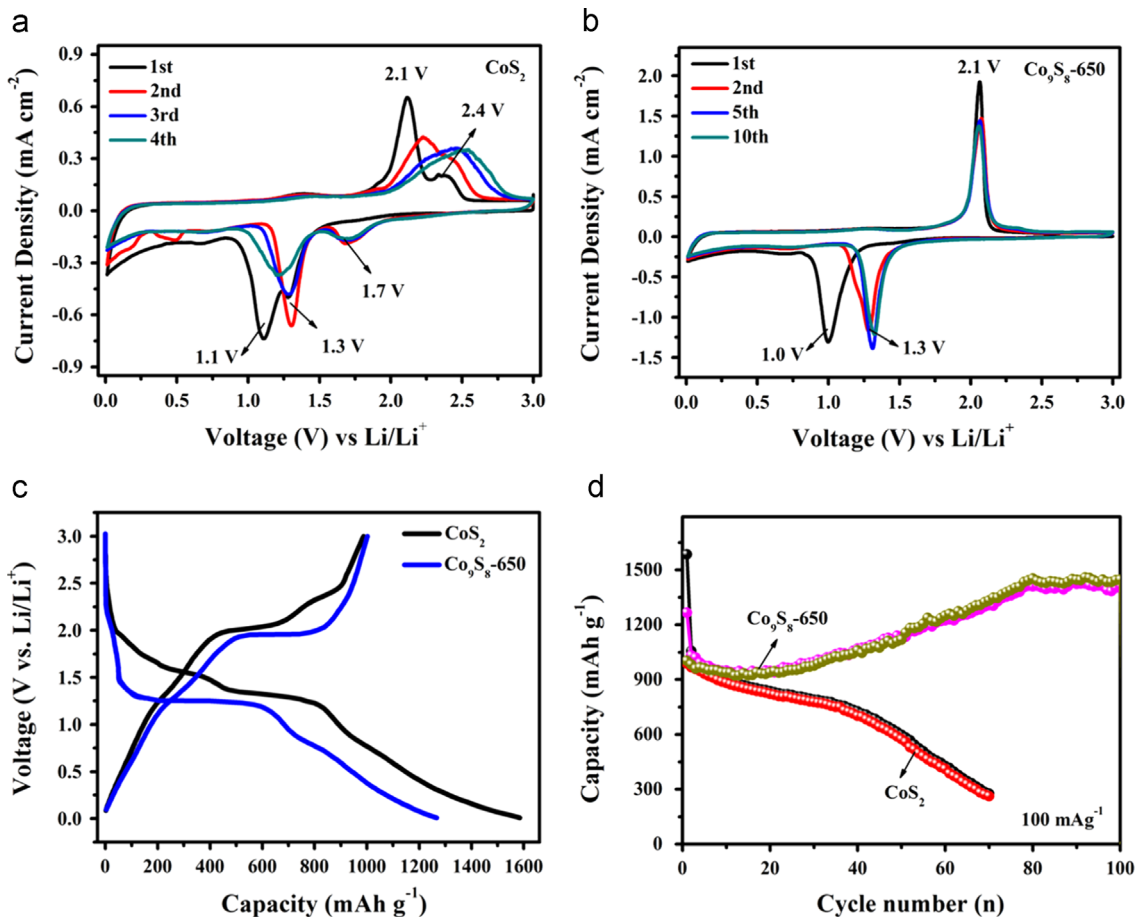


Figure 4 Cyclic voltammograms of the hollow nanospheres of (a) CoS₂ and (b) Co₉S₈-650. (c) The first discharge/charge profiles and (d) cycling performances of these two hollow nanospheres at 100 mA g⁻¹.

In order to clarify this point, Co₉S₈-650 is studied as a model to disclose the electrochemical nature of the capacity recovery. The capacity recovery in our case substantially arises from the voltage range of 0.01-1.4 V, as presented in Figure 5a. As proposed by Tarascon [45], the slope in this voltage range is related to the pseudo-capacitive behavior of a gel-like polymeric layer on the electrode surface. If so, the capacity recovery could be correlated to more and more pseudocapacitance upon cycling, which has not been suggested before. To verify this point, the electrode of Co₉S₈-650 is cycled between 0.01 and 1.8 V at different scan rates. As illustrated in Figure 5b, all the CV profiles show a nearly rectangular shape, a typical and important characteristic of a capacitive behavior [45]. Another strong indication for the pseudo-capacitive feature in this voltage range is given by the plots of current (i) at a fixed voltage against scan rates (ν) (Figure 5c). The linear relationship of i to ν confirms the capacitive feature of the electrode again. But in the routine measurements of anodes, the electrode is cycled over 0.01-3.0 V rather than 0.01-1.8 V. Then, more electrochemical reactions would be involved for the electrode, such as the lithiation/delithiation of active materials, the growth/dissolution of the polymeric film, and so on [45,47]. These reactions would lead to the structure reconstruction and the great increase of specific surface areas, providing more accessible active sites and increasing surface-related capacitance. The conclusion

is supported by the power law relationship between i_p and ν as follows [48,49]:

$$i_p = a\nu^b \quad (1)$$

where i_p is the peak current, ν is the scan rate, a and b are adjustable values. $b=0.5$ indicates that the peak current is diffusion-controlled, corresponding to a faradaic insertion/extraction reaction [50]. $b=1.0$ implies that the peak current is surface-controlled, indicative of a capacitive response [51]. In most cases, b locates between 0.5 and 1, suggesting a mixture of an insertion/extraction reaction and a capacitive response for the peak current. Closer to 1 b is, more capacitances in the peak current there are. Bearing these remarks in mind, b values of the cathodic peak currents are calculated for the electrode of Co₉S₈-650 at 2nd cycle, 10th cycle, 20th cycle and 50th cycle (Figure S4). As shown in Figure 5d, the b value of the peak current increase with cycle number from 0.65 at 2nd cycle to 0.78 at 50th cycle, confirming more and more capacitance upon cycling again.

After 100 cycles at 200 mA g⁻¹, the reversible capacity of Co₉S₈-650 is ~ 1122 mA h g⁻¹ (Figure S5), much better than the previous reports (Table S1) [7,15-28]. For example, rose-like Co₉S₈ microparticles assembled by numerous nanosheets [17], only showed a discharge capacity of 123 mA h g⁻¹ after 30 cycles at 50 mA g⁻¹. A similar structure of CoS with thick nanoplates as the building blocks exhibited a specific capacity of 302 mA h g⁻¹ after 25 cycles at 50 mA g⁻¹ [18]. Until

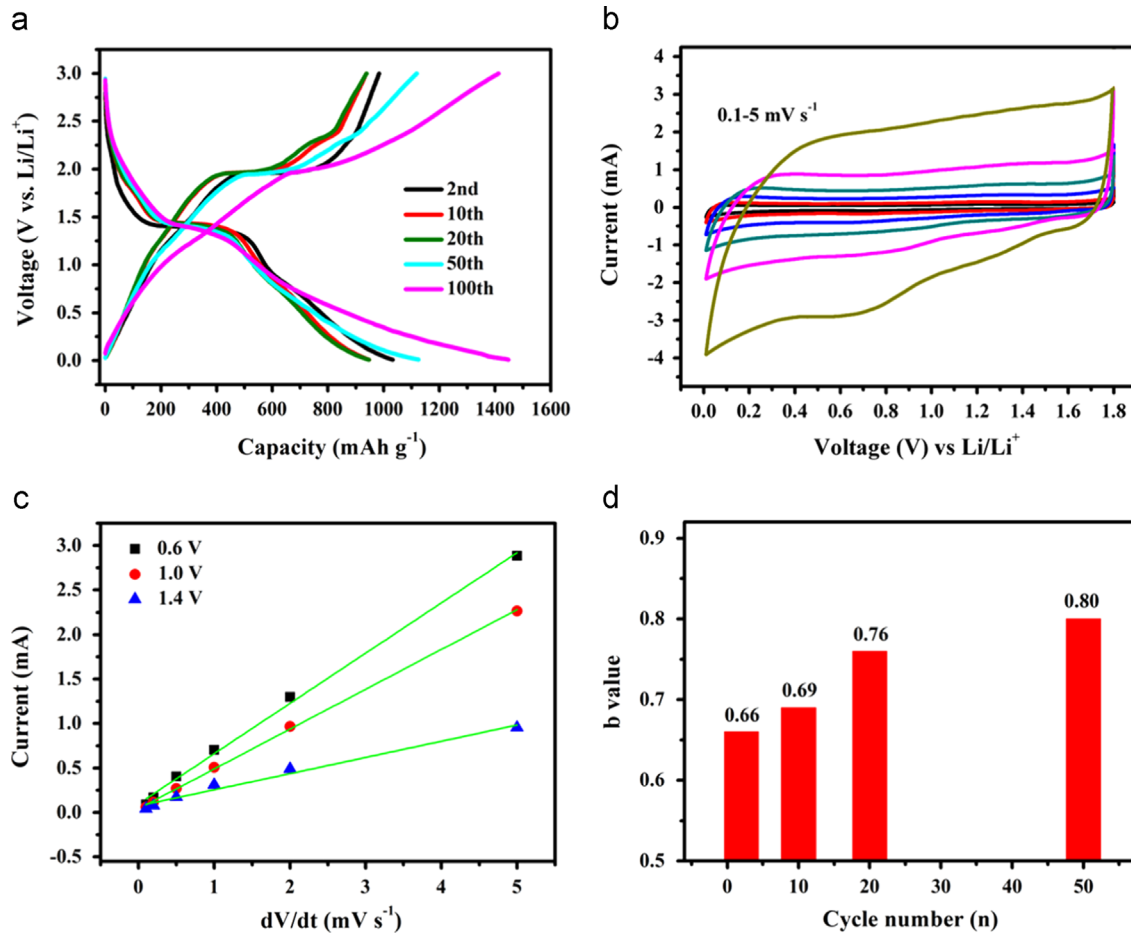


Figure 5 (a) Discharge/charge profiles of the hollow nanospheres of Co_9S_8 -650 for 100 cycles. (b) Cyclic voltammograms of these hollow nanospheres of Co_9S_8 -650 cycled over 0.01–1.8 V at different scan rates. (c) Plots of current (i) at 0.6, 1.0 and 1.4 V vs. scan rate (v). (d) The relationship of b values from the cathodic peak current (i_p) of the hollow nanospheres of Co_9S_8 -650 with cycle numbers.

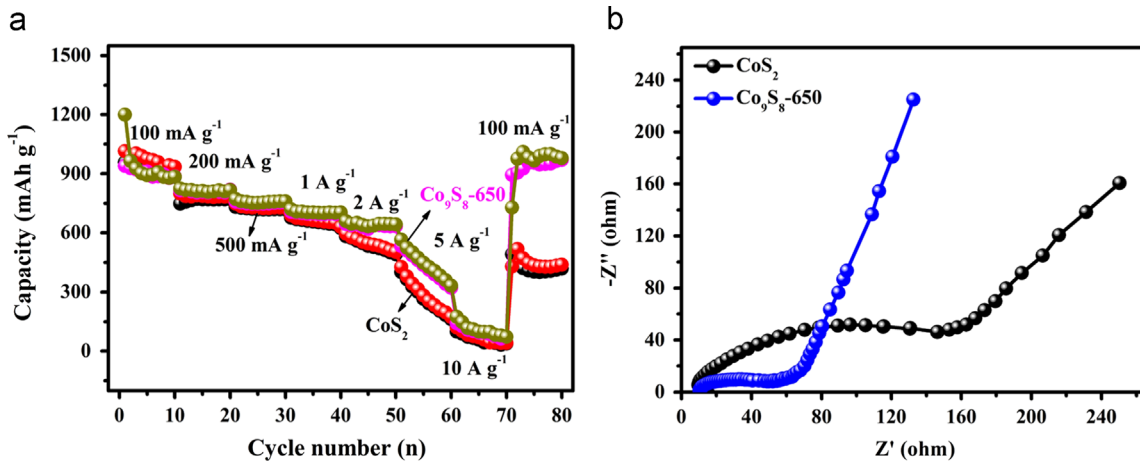


Figure 6 (a) Rate performances of the hollow nanospheres of CoS_2 and Co_9S_8 -650. (b) Nyquist plots of the hollow nanospheres charged to 3V after 50 cycles at 100 mA g^{-1} .

recently, the discharge capacity was enhanced to 485 mA h g^{-1} after 150 cycles at 100 mA g^{-1} by flower-like Co_{1-x}S particles prepared by a hydrothermal reaction [22]. It is believed that the excellent cycling stability of Co_9S_8 -650 could be associated with their hollow structure and nanoscale shell thickness, which has been documented for many transitional metal oxides

[14,52]. This good stability is directly supported by the SEM and TEM images of the electrode obtained after 50 cycles (Figure S6).

Figure 6a shows the rate capabilities of the hollow nanospheres of CoS_2 and Co_9S_8 -650. It is noteworthy that CoS_2 and Co_9S_8 -650 present close reversible capacities at

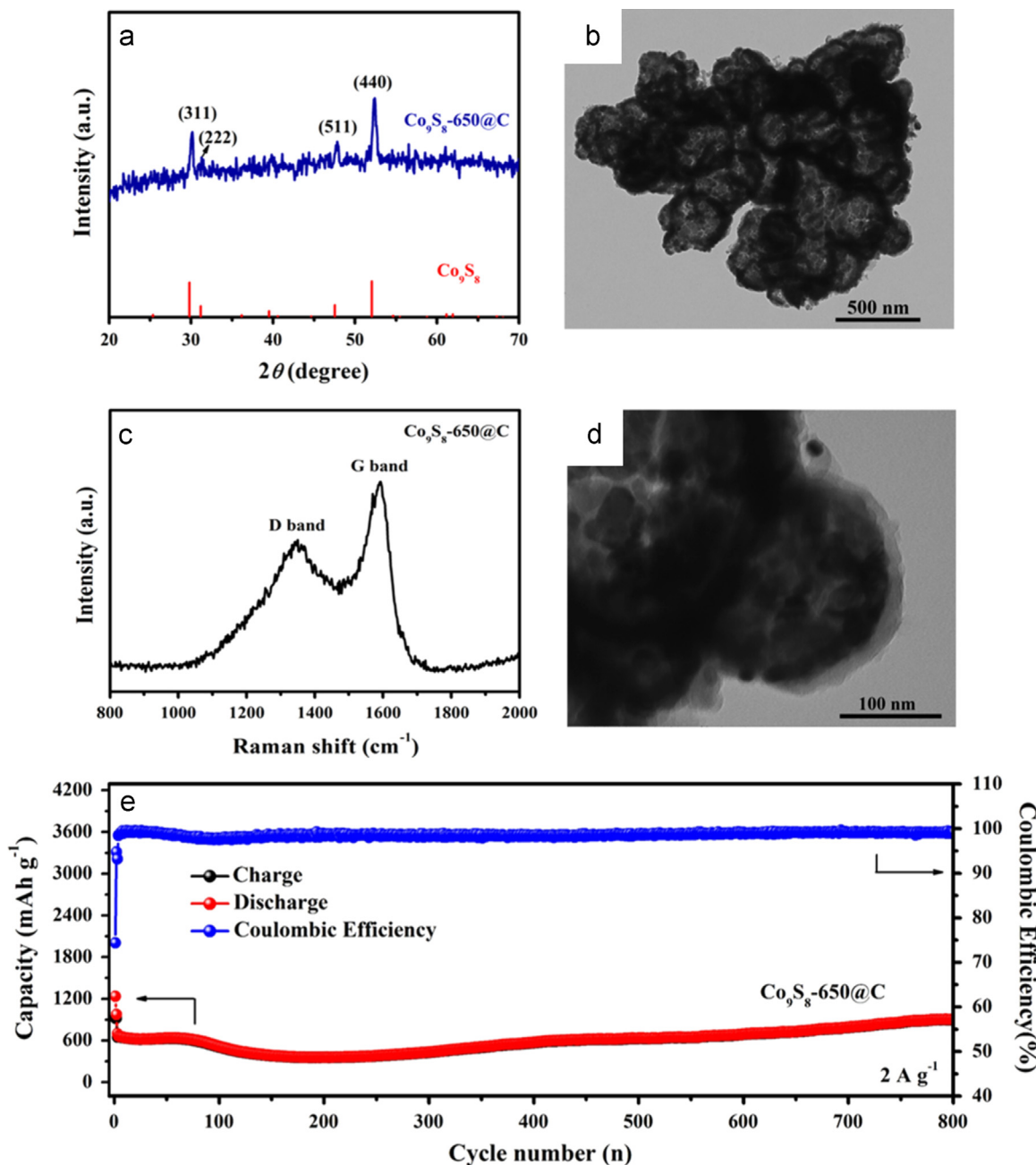


Figure 7 (a) XRD patterns, (b) TEM image, (c) Raman spectrum, and (d) magnified TEM image of the hollow nanospheres of Co₉S₈-650@C. (e) Cycling performance and coulombic efficiency of the hollow nanospheres of Co₉S₈-650@C over 800 cycles at 2 A g⁻¹.

low rates. At 0.1, 0.2, 0.5, 1, 2 and 5 A g⁻¹, the reversible capacities of Co₉S₈-650 are 904, 810, 751, 699, 635 and 426 mA h g⁻¹. After back to 100 mA g⁻¹, the reversible capacity of Co₉S₈-650 is recovered, which does not work for those of CoS₂ at all. This result implies the good electrochemical stability of Co₉S₈-650. Electrochemical impedance spectra (EIS) are measured to understand the excellent performances of the hollow nanospheres of Co₉S₈-650 from another viewpoint. As shown in Figure 6b, the Nyquist plots of the hollow nanospheres of CoS₂ and Co₉S₈-650 consist of a depressed semicircle at the high-to-medium frequencies connected to a slope at the low frequencies. The depressed semicircle represents the charge-transfer resistance (R_{ct}) between electrolyte and

electrodes. The slope is associated with constant phase element (CPE) from electrode. The phase angle of the slope for CoS₂ is close to 45°, suggesting a diffusion-controlled feature of lithium insertion/extraction. That of Co₉S₈-650 reaches 70°, indicating significant capacitive component in lithium insertion/extraction. Moreover, Co₉S₈-650 shows a smaller R_{ct} , benefiting the diffusion kinetics upon cycling.

Since carbon coating is regarded as one of effective strategies to improve the electrode performance in LIBs, the carbon-coated hollow nanospheres of Co₉S₈-650 are synthesized by a typical CVD process (Scheme 1). After the carbon coating, the product still keeps the hollow structure, nanoscale size and cubic-phase of Co₉S₈-650, as shown in Figure 7a-b. The successful formation of the carbon layer is confirmed by Raman

spectra and TEM images (Figure 7c-d). The CV curve of Co_9S_8 -650@C is almost identical to that of Co_9S_8 -650 (Figure S7), indicating similar electrochemical reactions. The reversible capacity can reach $\sim 1151 \text{ mA h g}^{-1}$ after 200 cycles at a current density of 500 mA g^{-1} (Figure S8), much higher than that of reported ones [7]. Even after 800 cycles at 2 A g^{-1} , the reversible capacity could be still maintained as $\sim 896 \text{ mA h g}^{-1}$ (Figure 7e). The excellent performances could be associated with the good charge-transfer kinetics, as revealed by the Nyquist plot in Figure S9. To the best of our knowledge, they are the best cycling performances for cobalt sulfides as anode materials for LIBs.

Conclusions

In summary, hollow nanospheres of amorphous CoS_2 are successfully synthesized by a facile solvothermal method. Then, the calcination of these hollow nanospheres in Ar/H_2 , gives rise to crystalline Co_9S_8 that preserves the hollow structure and size distribution of amorphous CoS_2 . The hollow nanospheres of Co_9S_8 obtained at 650°C exhibit the excellent performance, $\sim 1414 \text{ mA h g}^{-1}$ after 100 cycles at 100 mA g^{-1} , or $\sim 1122 \text{ mA h g}^{-1}$ after 100 cycles at 200 mA g^{-1} . After the carbon coating on the surface, the lithium-storage performances of Co_9S_8 could be further promoted to $\sim 896 \text{ mA h g}^{-1}$ after 800 cycles at 2 A g^{-1} . Another important result is that the capacity recovery upon cycling is attributed to the enhanced capacitive contribution caused by the repeated lithiation/delithiation processes.

Acknowledgments

This work was supported by 973 Project of China (No. 2011CB935901), National Nature Science Foundation of China (No. 91022033, 51172076 and 21471090), Shandong Provincial Natural Science Foundation for Distinguished Young Scholar (JQ201205), Independent Innovation Foundations of Shandong University (2012ZD007), and new-faculty start-up funding in Shandong University. We also thank Prof. Houyi Ma for helpful discussion.

Appendix A. Supporting information

Supplementary data associated with this article can be found in the online version at <http://dx.doi.org/10.1016/j.nanoen.2015.01.019>.

References

- [1] M. Armand, J.M. Tarascon, *Nature* 451 (2008) 652-657.
- [2] M. Winter, J.O. Besenhard, M.E. Spahr, P. Novak, *Adv. Mater.* 10 (1998) 725-763.
- [3] M.H. Liang, L.J. Zhi, *J. Mater. Chem.* 19 (2009) 5871-5878.
- [4] M. Wang, G. Li, H. Xu, Y. Qian, J. Yang, *ACS Appl. Mater. Interfaces* 5 (2013) 1003-1008.
- [5] B. Luo, Y. Fang, B. Wang, J. Zhou, H. Song, L. Zhi, *Energy Environ. Sci.* 5 (2012) 5226-5230.
- [6] N. Mahmood, C. Zhang, Y. Hou, *Small* 9 (2013) 1321-1328.
- [7] W. Shi, J. Zhu, X. Rui, X. Cao, C. Chen, H. Zhang, H.H. Hng, Q. Yan, *ACS Appl. Mater. Interfaces* 4 (2012) 2999-3006.
- [8] D. Zhang, Y.J. Mai, J.Y. Xiang, X.H. Xia, Y.Q. Qiao, J.P. Tu, *J. Power Sources* 217 (2012) 229-235.
- [9] N. Wang, L. Chen, X. Ma, J. Yue, F. Niu, H. Xu, J. Yang, Y. Qian, *J. Mater. Chem. A* 2 (2014) 16847-16850.
- [10] Y. Sun, X. Hu, W. Luo, F. Xia, Y. Huang, *Adv. Funct. Mater.* 23 (2013) 2436-2444.
- [11] Y. Xiao, X. Wang, W. Wang, D. Zhao, M.H. Cao, *ACS Appl. Mater. Interfaces* 6 (2014) 2051-2058.
- [12] Y. Su, S. Li, D. Wu, F. Zhang, H. Liang, P. Gao, C. Cheng, X. Feng, *ACS Nano* 6 (2012) 8349-8356.
- [13] L. Chen, H. Xu, L. Li, F. Wu, J. Yang, Y. Qian, *J. Power Sources* 245 (2014) 429-435.
- [14] J. Yue, X. Gu, L. Chen, N. Wang, X. Jiang, H. Xu, J. Yang, Y. Qian, *J. Mater. Chem. A* (2014) 17421-17426.
- [15] J.M. Yan, H.Z. Huang, J. hang, Z.J. Liu, Y. Yang, *J. Power Sources* 146 (2005) 264-269.
- [16] W. Luo, Y. Xie, C.Z. Wu, F. Zheng, *Nanotechnology* 19 (2008) 075602-075608.
- [17] R. Jin, J. Liu, Y. Xu, G. Li, G. Chen, *J. Mater. Chem. A* 1 (2013) 7995-7999.
- [18] Q. Wang, L. Jiao, H. Du, W. Peng, Y. Han, D. Song, Y. Si, Y. Wang, H. Yuan, *J. Mater. Chem.* 21 (2011) 327-329.
- [19] Y.N. Ko, S.H. Choi, S.B. Park, Y.C. Kang, *Chem. Asian J.* 9 (2014) 572-576.
- [20] Y. Gu, Y. Xu, Y. Wang, *ACS Appl. Mater. Interfaces* 5 (2013) 801-806.
- [21] Y. Wang, J. Wu, Y. Tang, X. Lu, C. Yang, M. Qin, F. Huang, X. Li, X. Zhang, *ACS Appl. Mater. Interfaces* 4 (2012) 4246-4250.
- [22] J. Wang, S.H. Ng, G.X. Wang, J. Chen, L. Zhao, Y. Chen, H.K. Liu, *J. Power Sources* 159 (2006) 287-290.
- [23] S. Liu, J. Wang, J. Wang, F. Zhang, F. Liang, L. Wang, *CrystEngComm* 16 (2014) 814-819.
- [24] Q. Wang, L. Jiao, Y. Han, H. Du, W. Peng, Q. Huan, D. Song, Y. Si, Y. Wang, H. Yuan, *J. Phys. Chem. C* 115 (2011) 8300-8304.
- [25] G. Huang, T. Chen, Z. Wang, K. Chang, W. Chen, *J. Power Sources* 235 (2013) 122-128.
- [26] B. Qiu, X. Zhao, D. Xia, *J. Alloys Compd* 579 (2013) 372-376.
- [27] R. Jin, J. Zhou, Y. Guan, H. Liu, G. Chen, *J. Mater. Chem. A* 2 (2014) 13241-13244.
- [28] Z. Li, W. Li, H. Xue, W. Kang, X. Yang, M. Sun, Y. Tang, C.-S. Lee, *RSC Adv* 4 (2014) 37180-37186.
- [29] Z.S. Wu, W. Ren, L. Wen, L. Gao, J. Zhao, Z. Chen, G. Zhou, F. Li, H.M. Cheng, *ACS Nano* 4 (2010) 3187-3194.
- [30] J.F.W. Mosselmans, R.A.D. Patrick, G. van der Laan, J.M. Charnock, D.J. Vaughan, C.M.B. Henderson, C.D. Garner, *Phys. Chem. Minerals* 22 (1995) 311-317.
- [31] F. Luo, J. Li, H. Yuan, D. Xiao, *Electrochim. Acta* 123 (2014) 183-189.
- [32] J. Gao, G. Liang, B. Zhang, Y. Kuang, X. Zhang, B. Xu, *J. Am. Chem. Soc.* 129 (2007) 1428-1433.
- [33] J.K. Chang, C.M. Wu, I.W. Sun, *J. Mater. Chem.* 20 (2010) 3729-3735.
- [34] A.M. Cao, J.S. Hu, H.P. Liang, W.G. Song, L.J. Wan, X.L. He, X.G. Gao, S.H. Xia, *J. Phys. Chem. B* 110 (2006) 15858-15863.
- [35] C.D. Wagner, W.M. Riggs, L.E. Davis, J.F. Moulder, G.E. Muilenberg, *Handbook of X-Ray Photoelectron Spectroscopy*, Perkin-Elmer Corporation, Eden Prairie, MN, USA, 1979.
- [36] Q. Liu, J. Zhang, *CrystEngComm* 15 (2013) 5087-5092.
- [37] A. Ghahremaninezhad, D.G. Dixon, E. Asselin, *Electrochim. Acta* 87 (2013) 97-112.
- [38] P. Poizot, S. Laruelle, S. Grangeon, L. Dupont, J.M. Tarascon, *Nature* 407 (2000) 496-499.
- [39] Q.Q. Xiong, J.P. Tu, S.J. Shi, X.Y. Liu, X.L. Wang, C.D. Gu, *J. Power Sources* 256 (2014) 153-159.
- [40] J.Z. Zhao, Z.L. Tao, J. Liang, J. Chen, *Cryst. Growth Des.* 8 (2008) 2799-2805.
- [41] Z.Y. Wang, J.S. Chen, T. Zhu, S. Madhavi, X.W. Lou, *Chem. Commun.* 46 (2010) 6906-6908.
- [42] S.H. Lee, Y.H. Kim, R. Deshpande, P.A. Parilla, E. Whitney, D.T. Gillaspie, K.M. Jones, A.H. Mahan, S.B. Zhang, A.C. Dillon, *Adv. Mater.* 20 (2008) 3627-3632.

- [43] A. Ponrouch, P.L. Taberna, P. Simon, M.R. Palacin, *Electrochim. Acta* 61 (2012) 13-18.
- [44] L. Su, Y. Zhong, Z. Zhou, J. Mater. Chem. A 1 (2013) 15158-15166.
- [45] S. Laruelle, S. Gruegeon, P. Poizot, M. Dolle, L. Dupont, J.M. Tarascon, *J. Electrochem. Soc.* 149 (2002) A627-A634.
- [46] H. Sun, G. Xin, T. Hu, M. Yu, D. Shao, X. Sun, J. Lian, *Nat. Commun* 5 (2014) 4526-4534.
- [47] S. Gruegeon, S. Laruelle, L. Dupont, J.M. Tarascon, *Solid State Sci.* 5 (2003) 895-904.
- [48] H. Lindstrom, S. Sodergren, A. Solbrand, H. Rensmo, J. Hjelm, A. Hagfeldt, S.E. Lindquist, *J. Phys. Chem. B* 101 (1997) 7717-7722.
- [49] J. Wang, J. Polleux, J. Lim, B. Dunn, *J. Phys. Chem. C* 111 (2007) 14925-14931.
- [50] A.S. Arico, P. Bruce, B. Scrosati, J.M. Tarascon, W.V. Schalkwijk, *Nat. Mater.* 4 (2005) 366-377.
- [51] B.E. Conway, V. Birss, J. Wojtowicz, *J. Power Sources* 66 (1997) 1-14.
- [52] B. Wang, J.S. Chen, H.B. Wu, Z. Wang, X.W. Lou, *J. Am. Chem. Soc.* 133 (2011) 17146-17148.



Yanli Zhou received her B.S. degree from Ludong University in 2009. Then she came to Henan University as a graduate student for M.S. degree. In 2012, she came to the School of Chemistry and Chemical Engineering at Shandong University to pursue her Ph.D. degree. Her thesis is related to the exploration of various sulfide nanostructures as anode materials for lithium-ion batteries.



Dong Yan received his B.E. degree from Shandong University in 2014. Currently, he is a graduate student at Institute of Process Engineering, Chinese Academy of Science.



Huayun Xu was awarded her B.S. degree from Qingdao University in 2002 and her Ph.D. degree from University of Science and Technology of China in 2007. During 2008-2009, she worked at Chonnam National University in Korea as a post-doctor. She joined in Shandong University of Science and Technology In 2009 and moved to Shandong University in 2010. Now, she is an assistant professor in the School of Chemistry and Chemical Engineering

at Shandong University. Her research interests is the fabrication of novel cathode materials for lithium-ion batteries and sodium-ion batteries.



Jinkui Feng received his Ph.D. degree in School of Chemistry and Molecular Science, Wuhan University in 2008. After that, he worked in the department of mechanical engineering at national university of Singapore as a postdoctor from 2008 to 2011. Then he came to Pennsylvania state university in 2011. He becomes an associate professor in the School of Material Science and Engineering at Shandong University from 2012. His research

interests focus on electrolytes and safety performances of lithium ion batteries.



Xiaolei Jiang received her B.S. degree from Zhoukou Normal University in 2011. She has become a Ph.D. student of Shandong University from then on. Her research interests are the development of polyanion compounds as cathode materials for Li⁺/Na⁺ ion batteries.



Jie Yue received her B.S. degree from Qufu Normal University in 2012. Then, she came to Shandong University as a graduate student. She has strong interests in syntheses of Mn-related and Tin-based nanostructures as anode materials for Li⁺/Na⁺ ion batteries.



Jian Yang received his B.S. and Ph.D. degrees from University of Science and Technology of China (USTC). Then, he worked as a post-doctor in National Taiwan Normal University, Singapore-MIT alliance, University of Washington (Seattle) from 2002 to 2007. In 2007, he was back to china as a full professor of South China University of Technology. He joined in the School of Chemistry and Chemical Engineering at Shandong University in 2011. His research interests are controllable synthesis of novel nanostructures targeted for electrochemical energy storage. So far, he has published more than 100 peer-reviewed articles on international journals.



Yitai Qian received his B.S. in chemistry from Shandong University in 1962. He was elected as an academician of Chinese Academy of Sciences in 1997. He presently is a Professor of University of Science and Technology of China, and he is also the director of the Key Laboratory of Colloid and Interface Chemistry (Shandong University), Ministry of Education. In 2008, he became a Fellow of Royal Society of Chemistry. Prof. Qian has published more than hundreds of refereed papers and several invited chapters. His efforts basically concentrate on solvothermal synthesis of inorganic nanomaterials.